PHYSICAL REVIEW B VOLUME 44, NUMBER 7 15 AUGUST 1991-I

Elastic scattering in ballistic-electron-emission-microscopy studies of the epitaxial $NiSi_2$/Si(111) interface

A. Fernandez, H. D. Hallen,* T. Huang, R. A. Buhrman, and J. Silcox
School of Applied and Engineering Physics, National Nanofabrication Facility and Materials Science Center, Cornell University, Ithaca, New York 14853-2501
(Received 26 April 1991)

We have fabricated epitaxial $NiSi_2$ films on Si(111) under ultrahigh-vacuum conditions and conducted *in situ* ballistic-electron-emission-microscopy (BEEM) measurements on this coherent interface system. We demonstrate the sensitivity of BEEM to mechanisms which broaden the angular distribution of the injected electrons for transport through a Si(111) interface. Spatially localized increases in ballistic transmission rates are observed, attributable to the elastic scattering of the injected electrons by structural defects present on the surface or buried in the silicide film.

Ballistic-electron transport in materials continues to be an important topic of research in solid-state physics as more sensitive techniques are developed for understanding this process and the fabrication of higher quality materials and devices continues to improve. The recent development of ballistic-electron-emission microscopy (BEEM) advances this capability by allowing the investigation of ballistic transport with nanometer scale spatial resolution.[1-5] The application of BEEM to epitaxial metal disilicide–silicon interfaces such as $NiSi_2$/Si(111) and $CoSi_2$/Si(111) is of particular interest due to the cleanliness and abruptness with which these interfaces can be grown. Recent experimental results[6] support detailed calculations[7] of ballistic transport properties for these interface systems, illustrating the effect of the complex band structure of these metals. In this paper, we report measurements on the epitaxial $NiSi_2$/Si(111) system which demonstrate that because the Si(111) interface has the conduction-band minimum offset from the zone center, BEEM is particularly sensitive to elastic scattering from structural defects present on the surface or buried in the silicide film. Specifically, defects are directly and strongly evident in the BEEM images as localized increases in ballistic transmission rates. This ability to study the effect of an isolated defect on electron transport represents a new and promising application of BEEM.

The BEEM technique is discussed in detail elsewhere.[1] Briefly, hot carriers are injected from the tip of a scanning tunneling microscope (STM) into a heterostructure sample. If the top layer is thinner than the inelastic mean free path, a significant fraction of these carriers can reach the interface without loss of energy. When the voltage on the tip is greater than the built-in potential at the interface, the carriers can cross the interface into the semiconductor. Here they are collected and measured by a high gain current amplifier attached to the back of the sample.

All BEEM measurements are conducted under ultrahigh-vacuum (UHV) conditions in a system described previously.[4,5] Epitaxial $NiSi_2$ films are grown following the well-established template method[8] and transferred in UHV directly to the STM chamber. Prior to Ni evaporation, the silicon is heated to 830 °C to drive off the surface oxide. Surfaces prepared in this manner display sharp (7×7) low-energy electron-diffraction patterns and no impurities can be detected by x-ray photoemission spectroscopy. Thin (~30 Å) single-crystal $NiSi_2$ films of type-*B* orientation are grown on *n*-type Si(111) wafers by deposition of 10 Å of Ni at room temperature followed by annealing at 550 °C. High-resolution transmission electron microscopy (TEM) studies of these interfaces show that they are indeed atomically abrupt, but structural defects such as misoriented grains are sometimes present as shown, for example, in Fig. 1.

In BEEM, the ballistic electrons that reach the metal-semiconductor interface are filtered in energy and momentum space as they cross the interface. Conservation of energy and transverse momentum laws, which strictly apply for coherent interfaces, allow transport into the semiconductor from only a fraction of the metal states. In the special case of a direct band-gap semiconductor, previous studies have established that a critical cone of acceptance, centered about the interface normal, is defined outside of which electrons are reflected back into the metal.[2]

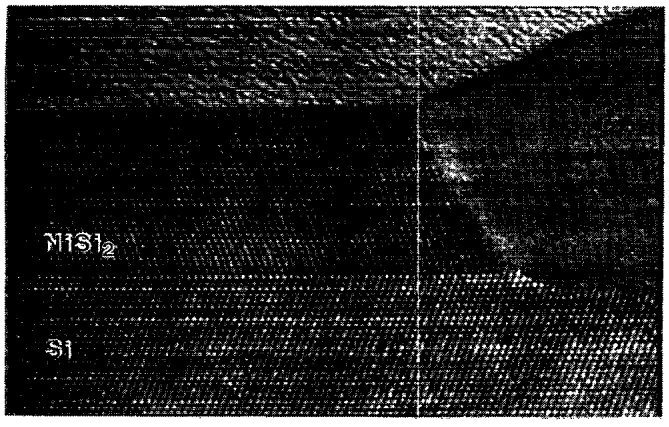

FIG. 1. High-resolution transmission electron micrograph of a type-*B* $NiSi_2$ film on Si(111) viewed in a $\langle 1\bar{1}0\rangle$ cross section. This particular film was grown following the template method, but additional Ni was deposited and annealed to produce a thicker film. The $NiSi_2$/Si(111) interface is abrupt and contamination free, but the presence of a misoriented grain is evident here.

We denote this type of system as a band-centered interface. Consider the more general case in which the conduction-band minimum (CBM) is offset from the zone center by an amount k_0 and that the principal axis of symmetry is tilted away from the interface normal by an angle α. For nonzero $\mathbf{k}_0$ and α, the projection of the CBM onto the plane of the interface does not fall at zero transverse wave vector; we call this type of system a band-offset interface. Such is the case for the Si(111) interface in which the six CBM are offset from the center along the ⟨100⟩ axes, tilted approximately 56° from the normal. Assuming parabolic bands in the semiconductor, the transverse momentum states allowed for transport across the interface lie within an annular region whose minimum and maximum are given by the following expression:

$$k_t = k_0 \sin\alpha \pm \left[\frac{2m_l e(V-V_b)}{\hbar^2} (\sin^2\alpha + \beta\cos^2\alpha) \right]^{1/2}, \quad (1)$$

where m_l and m_t are the longitudinal and transverse electron effective masses, respectively, $\beta = m_t/m_l$, V is the metal-tip bias, and V_b is the Schottky barrier height. The important fact distinguishing transport across a band-centered interface from transport across a band-offset interface is that for energies just above the CBM, there exist no states with near zero transverse wave vector in a band-offset system that satisfy transverse momentum constraints. For the Si(100) interface (i.e., $\alpha = 0$) the annulus defined above collapses to a circular region with a radius equal to $[2m_t(V-V_b)/\hbar^2]^{1/2}$ centered about $\mathbf{k}_t = \mathbf{0}$. Note that this condition is equivalent to having a band-centered system because the CBM is offset in a direction normal to the interface, and momentum conservation no longer applies in that direction. In a free-electron metal approximation, the derivation of a critical angle centered about the interface normal directly follows. The difference in transverse momentum constraints between the Si(111) and Si(100) interfaces is pictured schematically in Fig. 2. Comparison of BEEM measurements on Si(100) and Si(111) interfaces may reflect this difference, but the magnitude of the difference will depend heavily on the distribution of the electrons incident on the interface. Whereas phase-space constraints determine which states can cross an interface, the incident electron distribution determines the probability those states are occupied; thus both factors directly influence the magnitude of the transmitted ballistic current.

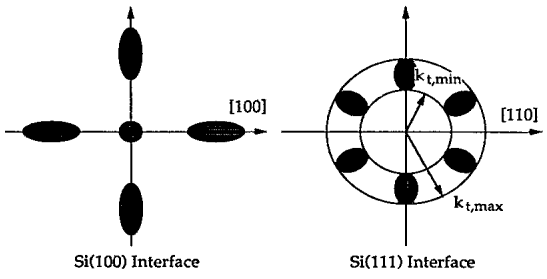

FIG. 2. Schematic representation in k space of the projection of the six Si conduction-band minima (CBM) onto the (100) and (111) interfaces. The transverse wave vectors of the incident electrons must lie within the shaded regions in order to satisfy energy and transverse momentum conservation laws and be allowed to cross the interface. It is clear from the diagram that for energies just above the CBM, electrons with near zero transverse momenta can cross a Si(100) interface but are reflected back into the metal at a Si(111) interface.

The momentum distribution of the electrons injected from the STM tip is strongly peaked in the forward direction, a consequence of the exponential dependence of the tunneling probability on the distance between the STM and the metal overlayer. The detailed shape of the distribution will depend on the vacuum tunneling conditions which include tip-sample separation, the metal and tip work functions, tip shape, and topography of the surface. Experimental uncertainty in these quantities makes a quantitative determination of the distribution difficult. Nevertheless, the principal angular dependence can be approximated via a planar tunneling theory[9] which gives the relationship,

$$P(E) \propto \exp(-\eta^2 t \sin^2\theta), \quad (2)$$

where θ is the polar angle from the normal, t is the tip-sample separation $\eta^2 = (2mE^2/\hbar^2\Phi)^{1/2}$, E is the electron energy, and Φ is the tunnel barrier. The probability decreases quickly with angle and, for typical values of the tunneling parameters,[10] is less than 5% by an incident angle of 20°. As a result, in the absence of scattering in the metal, the majority of the electrons incident on the interface will occupy states with transverse momenta near zero. For a band-offset interface, these electrons will be reflected back into the metal due to the lack of states near $\mathbf{k}_t = \mathbf{0}$ into which transport is allowed. Much lower ballistic transmission rates are, therefore, expected for transport through a Si(111) interface than through a Si(100) interface.

The magnitude of the collected current can be increased across the Si(111) interface if the ballistic electrons injected into the overlayer are scattered into states with larger transverse momentum before reaching the interface. Indeed, any mechanism which results in broadening the angular distribution will act to increase the density of electrons which satisfy the phase-space constraints and will thereby enhance transmission. With this in mind, examine the topographic and simultaneously recorded BEEM image of a type-B $NiSi_2$/Si(111) sample shown in Fig. 3(a) and Fig. 3(b), respectively. With this interface system, one might expect exceptionally uniform BEEM characteristics on the basis of the cleanliness and epitaxial quality of the interface. On the contrary, considerable spatial variation in collector current is often observed, as displayed in the BEEM image in Fig. 3(b). This variation nearly always takes the form of localized increases in BEEM current which vary in spatial extent from approximately 30–100 Å. Collector current versus sample-tip voltage spectra indicate that these increases are associated with an increase in the local ballistic transmission rate (the fraction of injected electrons which are collected) by a factor of typically 2 and not a shift in the Schottky barrier height. We propose that these enhanced regions are a signature for local broadening of the electron distribution by mechanisms occurring in the silicide film or at the

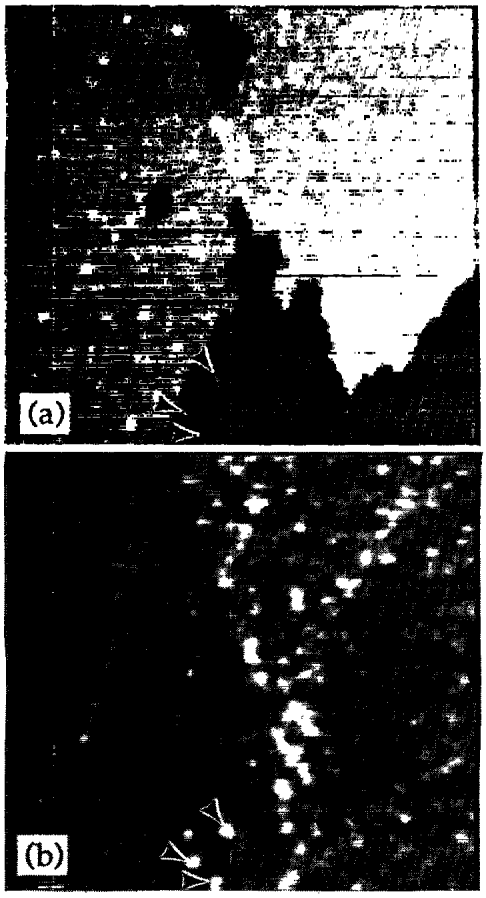

FIG. 3. STM and simultaneously recorded BEEM image of a type-*B* $NiSi_2/Si(111)$ sample. The 1800×1800-Å^2 scan was acquired with a sample-tip bias of 1.4 V and tunnel current of 1.0 nA. (a) STM topograph showing a single 3.14-Å step on the surface. The grey scale covers a range of 7.5 Å. (b) Corresponding BEEM image showing localized increases in collector current. A correlation exists between many of the adatom clusters visible in the topograph and the enhanced regions; three examples are indicated by the arrows. This correlation illustrates the sensitivity of BEEM to mechanisms which broaden the angular distribution of the ballistic electrons. The grey scale covers a range of 0–20 pA, and the average current over the scan is 8 pA.

silicide–silicon interface. Sensitivity to such mechanisms is a direct consequence of the offset of the Si CBM and the tight angular distribution of the injected electrons.

A clue to the physical mechanism which causes the distribution to broaden is that the regions of enhanced collector current are often correlated to adatom clusters present on the silicide surface. The STM topograph in Fig. 3(a) shows a single atomic step in the silicide surface with numerous single-atom high clusters distributed uniformly over the surface. The correlation of many of these clusters with enhanced regions in the BEEM image in Fig. 3(b) is indicated by the arrowed pattern. A possible explanation for this behavior is that localization of the tunneling electrons in small adatom clusters causes a dispersion of the electrons in momentum space as would be required by the Heisenberg uncertainty principle. But this effect will become important only for small cluster sizes on the order of several angstroms. The size of the clusters that correlate to enhanced regions is often greater than 40 Å, which is inconsistent with this explanation being generally applicable here. A more likely possibility is that the clusters are extended surface defects such as small stacking faults. Elastic scattering from these structural defects would result in an angular broadening of the ballistic electrons which is then detected as an increase in collector current.

More evidence that defects are imaged by BEEM in this manner is shown in the scan in Fig. 4. In this region, the surface topography [Fig. 4(a)] of the silicide film is no longer atomically flat over the entire area of the scan as in the previous scan. Instead, there is a large region in which the surface topography varies irregularly over a 26-Å height range, and it is clear that in this region the epitaxy

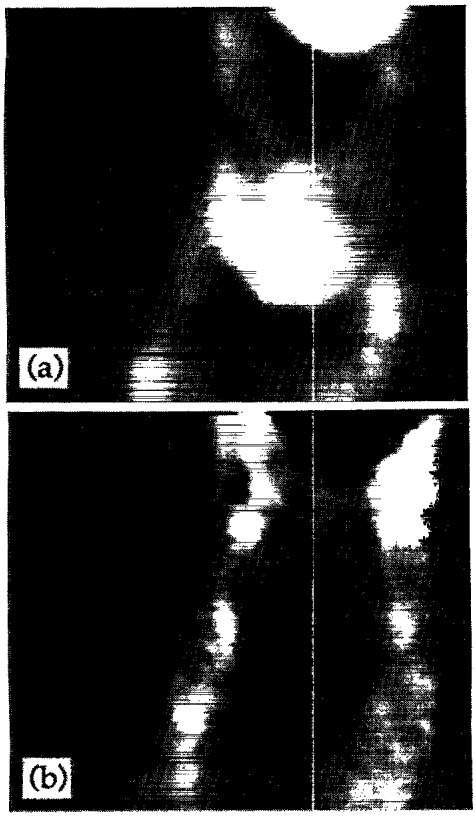

FIG. 4. STM and simultaneously recorded BEEM image of a type-*B* $NiSi_2/Si(111)$ sample. The scan area is 800×800 Å^2 and was acquired with a sample-tip bias of 1.8 V and tunnel current of 1.0 nA. (a) STM topograph displaying an area with a height variation that ranges over 26 Å. The rough topography indicates a region of poor epitaxial quality. The grey scale only covers a range of 14.6 Å so that the large mound at the top right-hand part of the scan is partially truncated. (b) Corresponding BEEM image showing a pronounced and continuous enhancement of ballistic transmission occurring at the perimeter of the region of poor epitaxy. Comparison of this scan and the TEM micrograph in Fig. 1 suggests that this region is a misoriented $NiSi_2$ grain. The enhanced transmission is caused by elastic scattering of the ballistic electrons at the grain boundary. The grey scale covers a range of 0–110 pA.

is no longer ideal. A pronounced and continuous stretch of enhanced collector current, visible in the BEEM image in Fig. 4(b), borders this region which once again implies that the electron distribution is locally broadened here. High-resolution TEM has revealed the presence of misoriented grains in these films as shown in the micrograph in Fig. 1. It is evident that part of the silicide film (the left-hand side of the micrograph) is perfectly aligned with the underlying Si lattice since the $[1\bar{1}0]$ columns are resolved both above and below the interface. On the right-hand side, however, the columns are no longer visible, although the (111) lattice planes are still resolved. The simple interpretation is that this region of the silicide film is still epitaxial but is rotated slightly with respect to the Si lattice about the [111] axis. The grain boundary that borders the oriented and misoriented regions of the film is clearly visible. Comparison of this micrograph with the scan in Fig. 4 strongly suggests that the region of poor epitaxy imaged in this scan is, in fact, a misoriented part of the film. Elastic scattering of the injected electrons would be expected as the STM were scanned across the grain boundary and a corresponding increase in transmission rates would result. Away from the boundary, transmission rates would fall to normal values. This is exactly what is observed in the BEEM image. In addition, the rise in topography seen in the STM image is consistent with the increase in silicide thickness evident in the TEM micrograph where the film is misoriented.

In conclusion, we have shown through measurements on the epitaxial $NiSi_2Si(111)$ system the sensitivity of BEEM to mechanisms which broaden the angular distribution of the injected carriers when transport is through a band-offset interface system. Correlations between structural defects in and on the silicide film and local increases in collector currents suggest that elastic scattering is a primary mechanism responsible for the spatial variation in the BEEM current. Of course, structural defect scattering is not necessarily the sole origin of the strong heterogeneity seen in the BEEM image for this epitaxial system. Other scattering mechanisms may also be present and thus also may serve to broaden the momentum distribution, while interface state defects could possibly be nonuniformly modulating the interfacial ballistic transmission. However, the strong effect of structural defects is clear. In principal, sensitivity to elastic scattering from individual point defect states in the overlayer or at the interface is possible, although spatially resolving such point defect states may be difficult to attain experimentally. Nonetheless, the ability to study the effects of particular defects on hot carrier transport opens up another application for BEEM which shows increasing potential as an interface and film transport characterization tool.

The authors wish to thank Kaikee Wong for performing the TEM studies shown here. Research support was provided in part by the Office of Naval Research and the Semiconductor Research Corporation. Initial support was also received from the National Nanofabrication Facility and the Cornell Material Science Center which are supported by the National Science Foundation. A.F. acknowledges support provided by the Hertz Foundation and H.D.H. acknowledges support provided by IBM during a portion of this research.

---

*Present address: AT&T Bell Laboratories, Murray Hill, NJ 07974.

[1]W. J. Kaiser and L. D. Bell, Phys. Rev. Lett. **60**, 1406 (1988).

[2]L. D. Bell and W.J. Kaiser, Phys. Rev. Lett. **61**, 2368 (1988).

[3]A. E. Fowell, R. H. Williams, B. E. Richardson, and T.H. Shen, Semicond. Sci. Technol. **5**, 348 (1990).

[4]A. Fernandez, H. D. Hallen, T. Huang, R. A. Buhrman, and J. Silcox, Appl. Phys. Lett. **57**, 2826 (1990).

[5]A. Fernandez, H. D. Hallen, T. Huang, R. A. Buhrman, and J. Silcox, J. Vac. Sci. Technol. B **9**, 590 (1991).

[6]W. J. Kaiser, M. H. Hecht, R. W. Fathauer, L. D. Bell, and E. Y. Lee (unpublished).

[7]M. D. Stiles and D. Hamann, Phys. Rev. Lett. **66**, 3179 (1991).

[8]R. T. Tung, J. M. Gibson, and J. M. Poate, Phys. Rev. Lett. **50**, 429 (1983).

[9]E. L. Wolf, *Principles of Electron Tunneling Spectroscopy* (Oxford Univ. Press, New York, 1985), Chap. 2.

[10]Typical tunneling parameters: 10 Å sample-tip distance, 3.5-eV tunnel barrier and 10-eV electron energy.